CFSRC COLLOQUIUM

Proceedings of the Cold-Formed Steel Research Consortium Colloquium
17-19 October 2022 (cfsrc.org)

Structural Performance of Cold Formed Sections Portal Frames Eave Connections with Different Fasteners (Screws / Bolts)

Sherif A. Mourad [1], , M.T.Hanna [2], Hazem H. Elanwar [1] , Ahmed Massoud [3]

Abstract

Recently, there is a growing interest for cold formed sections to be used in low- to mid-rise buildings as primary load carrying structural elements as well as portal frames with short spans. This paper studies the structural behavior of cold formed sections portal frames eave connections under vertical static loads. In the connection details, the beams and columns are connected together via tapered gusset plates. Two types of fasteners are studied which are self-drilling screws and bolts. The beam and column sections are back-to-back lipped channels with web, flange, and lip dimensions are 200mm, 60mm, and 20mm; respectively. Thickness of the sections is kept constant equal to 2mm. Parameters studied are thickness of the gusset plate (2mm, and 3mm). The connections are investigated experimentally as well as numerically using ABAQUS software. In the finite element simulation, 4-noded reduced integration shell elements (S4R) are used for modelling the steel sections, and a bi-linear stress-strain curve is adopted. The material properties are defined based on a tensile coupon test result. Moreover, both bolts and screws are modeled as elastic-rigid fasteners. Mechanical properties of the screw fasteners were defined according to direct shear tests of lap joint with single screw. Results reveal that, experimental as well as numerical findings are comparable. In addition, failure modes are either bearing and screw tilting in the gusset plates or local buckling in the gusset plates. Further, for thick gusset plates, bolted connections exhibit high strength accompanied with small vertical displacements compared with the screw connections.

1. Introduction

Cold-formed steel (CFS) has been commonly used as secondary load-carrying structural elements such as wall girts, roof purlins, cladding and stud walls. Recently, there is a growing interest for CFS sections to be used in low- to mid-rise buildings as primary load carrying structural elements as well as portal frames with short spans [1]. CFS offers a wide range of advantages such as higher flexibility in obtaining the required cross-sectional shapes due to its small thicknesses, high strength-to-weight ratio compared to hot-rolled members, therefore, easier to transport and handle on site [1][2].

Previous work studied the flexural capacity of the CFS sections and its influence on the behavior of portal frames. Rasmussen [3] studied the effect of bi-directional moment on the flexural capacity of the CFS sections using Direct Strength Method (DSM) design approach [4],[5]. The results showed that the elastic local buckling moment is decreased by 36.3% when the bi-directional moment was included. Bi-directional moment can occur to CFS section from eccentricity of shear center for single C- sections [6]. Bhavitha et al. [7] studied the effect of using perforated CFS box sections, as means of reducing the own-weight of the system, on the performance of beam-to-column bolted moment connections, while Liu et al. [8] tested ten specimens to investigate the behavior of sigma section in sleeve connection. Ye et al. [9] investigated the efficiency of using rounded flange and folded flange CFS sections. Folded flange sections resulted in higher ductility levels with the same beam slenderness ratio and bolt arrangement compared to the curved, flat, and stiffened flat sections, respectively.

Several research have focus on beam-to-column moment connections for CFS portal frames with short to medium spans. Hanna et al. [10] investigated the load-carrying capacity of CFS beam-to-column moment connections using screw joints and compared the results with bolted joints. Ten specimens were tested, and FE models were developed for these specimens where it was found that the gusset plate thickness did not significantly affect the final capacity of both types of connections while bi-moment took place as the CFS section buckled. Serror and Hassan [11] showed that beam-to-column connections experience

[1] Professor, Structural Eng. Dep., Faculty of Engineering, Cairo Uiversity, Egypt, smourad@eng.edu.eg
[2] Professor, Stucture and Metallic Construction Dept. Housing and Building National Research Center, Egypt, m_tawfick2003@yahoo.com
[3]Teaching Assistant, Faculty of Engineering, British University in Egypt, BUE, ahmed.massoud@bue.edu.eg

instability before reaching the profile moment capacity. Therefore, it is reasonable to use out-of-plane stiffeners to delay the premature buckling and decreases the overall stress. The study showed that an increase in strength and stiffness can reach up to 15% and 115 % relative to the un-stiffened specimens, respectively. Full scale CFS portal frames have been adopted in multiple researches [12] - [15] while other researches also focused on testing the apex, eave and base connections of the portal frames where different parameters such as bolts and stiffeners arrangement, were investigated [16][17]. Rasmussen [18] performed a series of analyses and connection tests to examine the flexural behavior of apex, eave, and base connections for cold-formed steel single C-section portal frames. Simplified nonlinear FE analysis were presented to develop moment-rotation relations and the associated flexural stiffness values for these connections were derived. The results showed that the bending of the eaves' brackets and collapse were caused by the screw fracture, whereas the apex connections failed owing to the inelastic local buckling of one of the C-sections' compression flange-web junction.

2. Experimental Setup

Specimens tested consist of cantilever beams connected to columns through gusset plates as illustrated in Figure 1. Both beams and columns have back-to-back cold formed lipped channel sections with nominal dimensions of 200, 60, 20 for web depth, flange width, and lip depth; respectively. The nominal section thickness is 2mm. The vertical height of the column from the base plate to the centerline of the beam is 1000mm. The horizontal length of the beam from the load application to the centerline of the column is 1000mm. Arrangements of the fasteners (screws / bolts) are as indicated in Figure 1. Three specimens were tested where self-drilling screws of diameter 6 mm were used for the connection, while two specimens were tested using ordinary bolts of diameter 12 mm. The results of the bolted and screw-fastened connections will surely differ as bolts' diameter are two times that of the screw-fastened connections, however, the aim is to compare the behavior of these two types of connections to monitor the performance of self-drilling screws. Two screw-fastened specimens used an additional top plate connecting the column's outer flanges with the beam's top flanges.
The effect of the added top plate on the moment-rotation behavior is investigated in this research. Furthermore, two 40 x 4 angles were used as stiffeners for the gusset plate as shown in Figure 1. where buckling of the gusset plate is expected. Small clearance between the top of the column and the bottom flanges of the beam was made to allow the beam to rotate without bearing on the column. Table 1 lists the measured dimensions of the tested specimens.

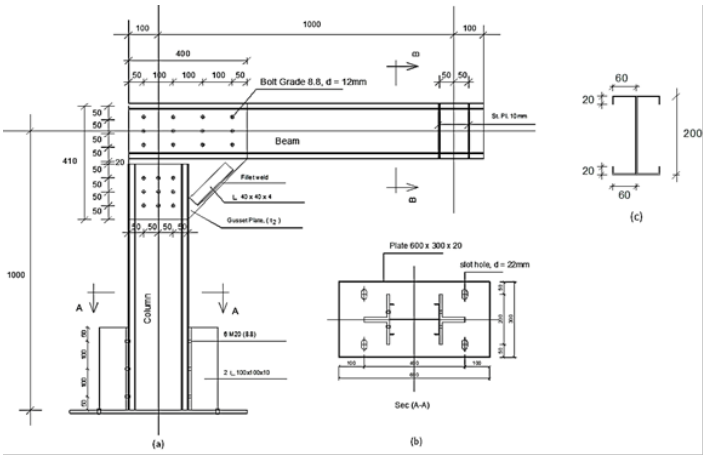

Figure 1: (a) Schematic drawing for beam-to-column connection (S2, S2') (b) base plate detail (c) CFS section dimensions

Table 1: Measured Dimensions of the specimens

Specimen	Section Dimensions (mm)				Specimens Dimensions (mm)	
	Web Depth, H	Flange width, B	Lip Depth D	Thickness, t	H	L
P. S	200	60	20	3	882	1001
S1					881	1002
S2					881	1001
S1'				2	883	1002
S2'					883	1002

2.1 Material Properties

Three coupons were extracted from the material from which the specimens were manufactured. Dimensions of the coupons and the test procedure were according to the ASTM-A370 specifications. Summary of the results are listed in Table 2. Average of yield stresses, and ultimate stresses, are 350 MPa, and 450 MPa; respectively. The percent elongation in 50mm elongation is 22.14%. Moreover, direct shear tests were performed on three screw-fastened steel plates to determine the maximum shear strength that could be carried by the screw. The screw is formed of a single hex-washer head of diameter equals 6 mm. Steel plates of 2 mm thickness, 50 mm width and 200 mm depth were used with screw edge distance equals 50 mm. The failure mode observed for the three specimens was tilting and bearing in plate as shown in Figure 2. Failure took place at an ultimate stress in the screw equal to 720 MPa.

Table 2: Measured Dimensions of the specimens

Specimen	Yield strength (N/mm2)	Ultimate Strength (N/mm2)	Elongation (%)
SP01	324.87	419.63	21.02
SP02	356.91	457.07	21.04
SP03	365.48	470.87	24.37

a) Test specimen b) Specimen in the test machine c) Failure shape

Figure 2: Shear test of the screws

2.2 Test setup and procedure

Specimens are placed vertically in the test machine as showed in Figure 3. Columns are connected to 10mm thickness base plate through vertical angles (100x100x10). These angles are welded to the base plate and connected to the specimen's column flanges by 12 bolts M16. In turn, the base plates are fixed in rigid beam by bolts. Slot holes in the base plate were done to allow proper lateral adjustment of the specimen. This configuration insures the fixed base condition of the specimens. Loads are applied to the specimens vertically through 20-ton jack. The connection between the jack and the beam allows free in-plane rotation of the beam at this point while preventing lateral movement. To prevent the out of plane displacements of the tested specimens, lateral supports are provided at the points of load application and beam mid-length by means of rigid frame Figure 5(a). This frame placed in plane perpendicular to the plane of the specimens, and it consists of vertical UPN columns connected by horizontal plates. Spacing between columns allows the specimen to pass through. In this frame the specimen restricted between two vertical plates, to prevent the out of plane displacements. To minimize friction between plates of the lateral support in contact with the specimens, a lubricant has been placed Figure 5(b). The test frame and the lateral support systems are illustrated in Figure 4.

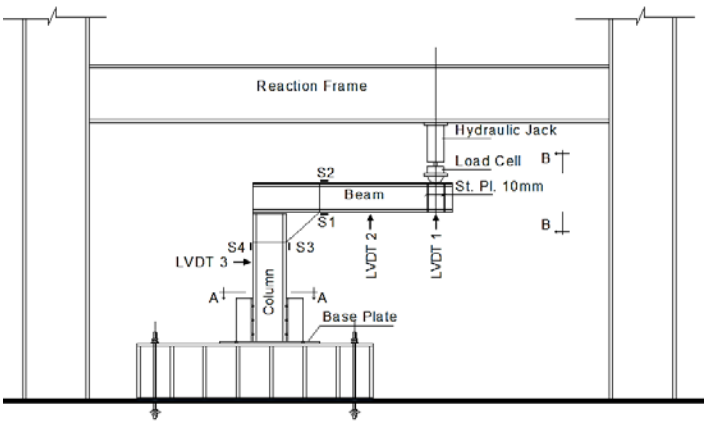

Figure 3: A schematic showing the test configuration

Figure 4: Actual configuration of the specimen

(a) (b)

Figure 5: (a)Steel lateral support (b)lubrication between the support and flange plates

The in-plane deformations of the specimens were measured through linear variable displacement transducers (LVDT)

with accuracy of 0.01 mm. The measured points were the vertical displacements of the beam end section below the load application (LVDT 1), as well as the beam mid-length section (LVDT 2). In addition, the horizontal displacement of the mid-height section of the column was recorded (LVDT 3) as showed in Figure 3. The LVDT readings were collected using a data acquisition system. In addition, four strain gages were attached to the specimens to measure the tension as well as the compression flange strains at sections just before the connection in the specimen beam column as showed in Figure 3. An arbitrary increment of load equal to 5 KN was applied, and then the load was held constant until stable readings were recorded. This procedure was applied for each additional load in a repetition form increment until excessive deflections were observed with no change or increase in the applied load. Thus, the ultimate load was reached.

3. Finite Element Model

Numerical models were developed where both geometric and material non-linearities were considered using ABAQUS software [19]. The model simulated all loading points, boundary conditions, surface interactions and constraints as presented in the experimental program. The basic parameters of the numerical model are as follows: 4-noded reduced integration shell elements (S4R) were used for modelling the steel sections with mesh size of 10 mm x 10 mm from a sensitivity analysis. Material properties were defined based on the coupon tensile test results, however, bi-linear stress-strain curve was adopted. The yield stress, Fy, equals 350 MPa, ultimate stress, Fu, equals 450 MPa, modulus of elasticity, E, equals 210 000 MPa, and Poisson's ratio, υ, equals 0.33.

Both bolts and screws were modeled using the discrete point-based fasteners feature instead of physically modelling the screws and bolt holes. It was noticed from the experimental work that no plastic deformations or failure were observed in the bolts, therefore, bolts were modelled as elastic-rigid fasteners, while properties of the screw fasteners were defined according to the mechanical properties obtained from the experimental data. The axial stiffness of the screws was taken as 1 kN/mm according to the experimental work performed by Wrzesien [20].

4. Results and Discussion

4.1 Experimental tests results

A total of 5 specimens were tested using displacement-controlled, monotonic loading. Three specimens were screw-fastened beam-to-column moment connections while the remaining two were bolted. A pilot specimen (PS) was tested Figure 6 to monitor the behavior and flexural capacity of these types of connections and calibrate the numerical models against the experimental test results. The load-displacement curve of the PS is illustrated in Figure 7 where the maximum load reached was 13 kN. Afterwards, a different lateral support was manufactured and used for the following specimens.

Figure 6: Pilot Specimen (PS) (a)Configuration and testing (b)Deformed shape of PS

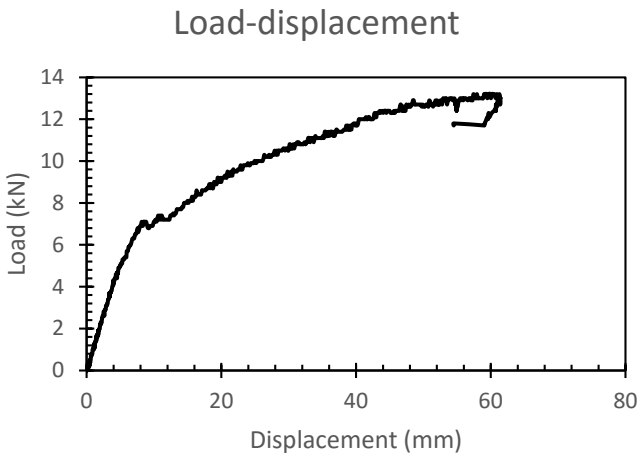

Figure 7: Load-displacement curve for Pilot Specimen (PS)

Figure 8: Deformed shape for S1 specimen

Specimen S1 was tested by using the steel lateral support, as shown in Figure 8. A spot welding between the gusset plate and the beam, and between the gusset plate and the column was used for erection purposes which affected the behavior of the connection providing extra strength and rigidity. Specimen S1' is the same as S1, illustrated in Figure 9(a), after making sure to remove any spot welding, moreover, the thickness of the gusset plate is 2 mm instead of 3 mm. It was noticed that the failure mode was local buckling in the gusset plate Figure 9(b), with ultimate load equal to 9.3 KN and a displacement equal to 161.8 mm, as illustrated in the load-displacement curve in Figure 10.

(a) (b)

Figure 9: Specimen S1' (a) testing (b) Deformed shape

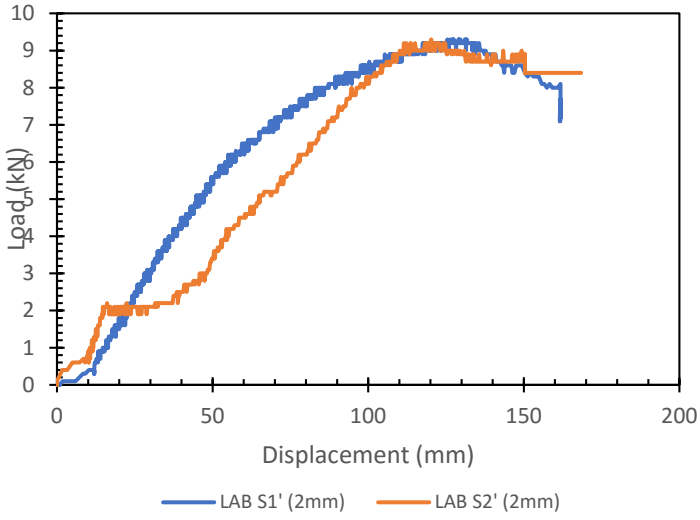

Figure 10: Load-displacement curves for S1' and S2'

Specimen S2 is similar to S1 and S1'; however, steel bolts were used instead of self-drilling screw. Spot welds were also used between the column, beam, and the gusset, which changed the failure behavior. The failure mode was tearing in the gusset plate, as shown in Figure 11, at an ultimate load equal to 14.1 KN and displacement equal to 10 mm. As shown in Figure 12, the effect of the spot welding gives the specimen large stiffness in the beginning until it reaches 10.5 KN then the spot welding failed, and the specimen starts to gain strength more with time.

Figure 11: Tearing in the gusset plate observed in S2

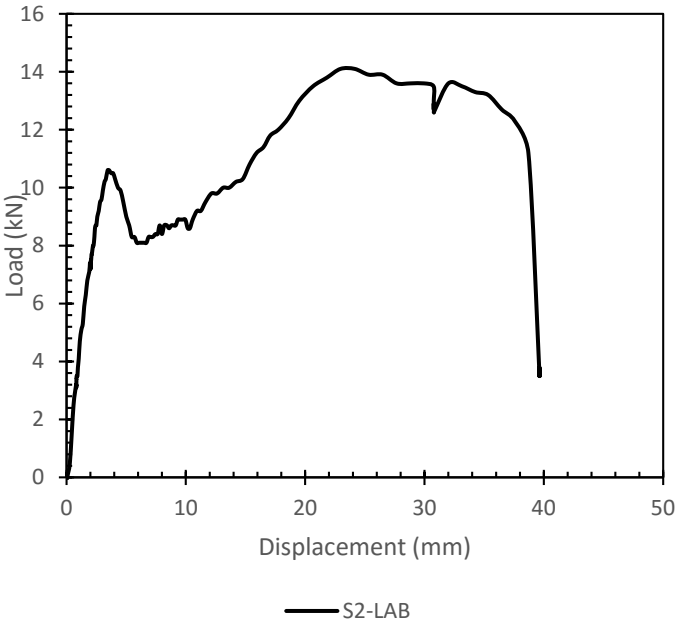

Figure 12: Load-displacement curve for S2

Specimen S2' is the same as S2 but also without spot welding, as seen in Figure 12(a). The failure mode was buckling in the gusset plate as seen in Figure 12(b) with an ultimate load that equals to 9.3 kN and maximum displacement equal to 168.4 mm. Comparing it to S2, S2' demonstrated that the load has been decreased and displacement increased because there was no welding in the specimen as showed in Table 3. Also, the failure

changed from tearing in the gusset plate to buckling in the gusset plate.

(a) (b)

Figure 13: (a)Test setup for S2' (b) Deformed shape for S2'

Table 3: A Summary of the experimental results

Specimen	Ultimate load (KN)	Deflection (mm)
PS	13.2	61.5
S1	11.2	99.4
S1'	9.3	161.8
S2	14.1	100
S2'	9.3	168.4

4.2 Numerical Model Verification

For specimen S1', it could be observed for the laboratory test that the mode of failure was buckling in the gusset plate, which is in agreement with the model outcome, as shown in Figure 14 and Figure 15. Regarding the force-displacement relationship, the specimen reached 10.7 kN in the finite element model and 9.2 KN in the experimental test with a variation of 14 %. While the deflection of the finite element model is equal to 134 mm, and the experimental test is equal to 132 mm with a variation of 1.4 %, as seen in Figure 16. It can also be noticed from Fig. 16 that the finite element model and the experimental test are good agreement with slight increase in strength recorded by the FE model.

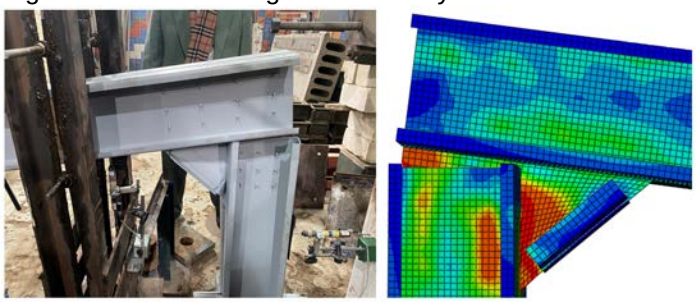

Figure 14: In-plane buckling for gusset plate

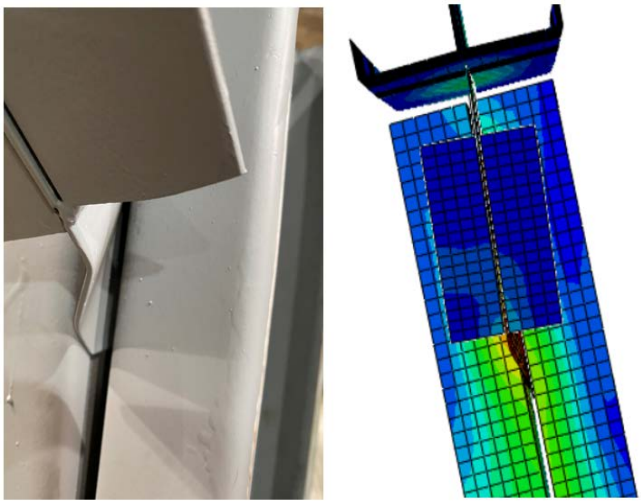

Figure 15: Side view for gusset plate of specimen S1'

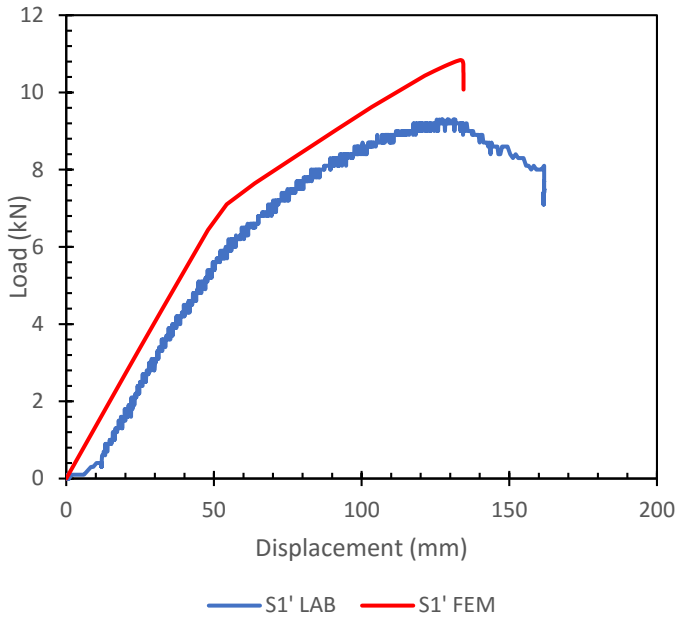

Figure 16: Load-displacement curve for S1' (Lab vs. FEM)

For specimen S2', it was observed that the mode of failure was buckling, which happened in both the finite element model and the lab specimen at the gusset plate, as shown in Figure 17, Figure 18 and Figure 19. The specimen reached 11.7 kN in the finite element model and 9.3 kN in the experimental test, with a variation of 20.5%. While the deflection of the finite element model is equal to 125 mm, and the experimental test is equal to 121 mm with a variation of 3.2%. As shown in Fig. 20, the FE model gave similar behavior to the lab. specimen, however, the FE model gave higher values in terms of strength.

Figure 17: Deformed shape for Specimen S2' (Lab vs. FEM)

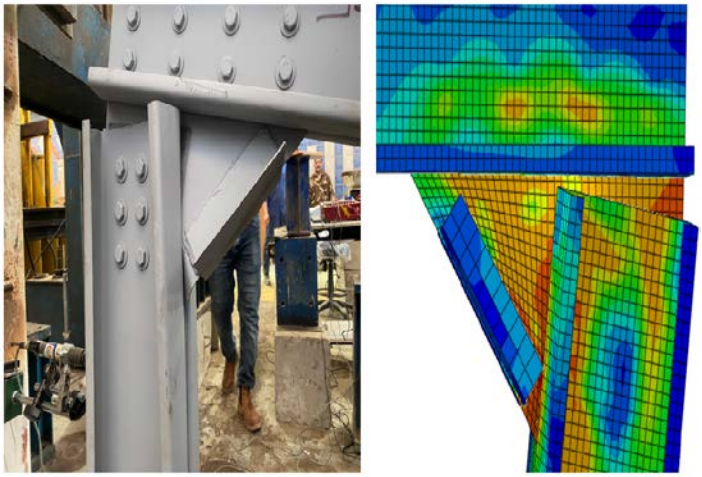

Figure 18: In-plane buckling for gusset plate in Specimen S2' (Lab vs. FEM)

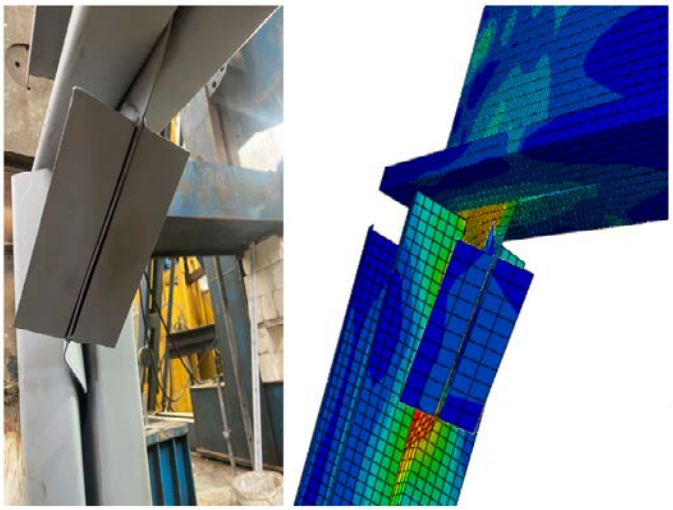

Figure 19: Side view for gusset plate buckling in specimen S2' (Lab. vs. FEM)

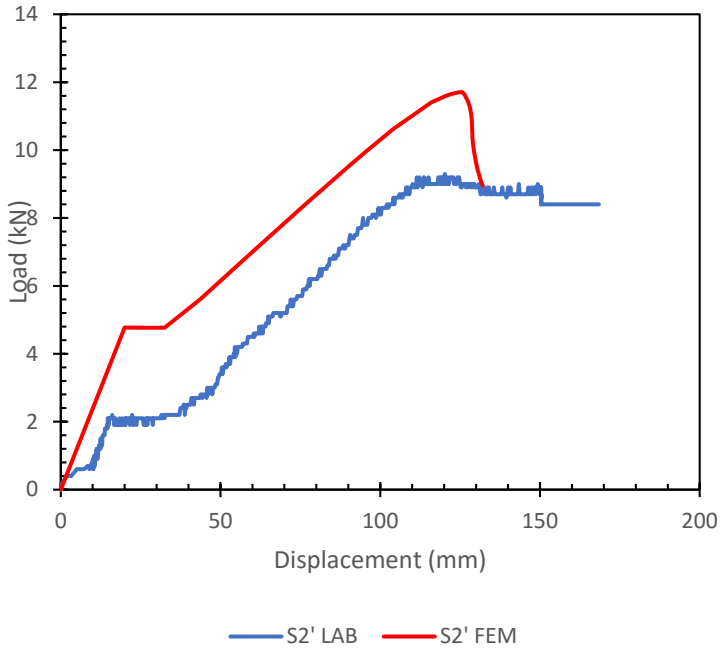

Figure 20: Load-Displacement curve for S2' (LAB vs. FEM)

Table 4: Comparison of load values between experimental and FEA results at ultimate load

Specimen	Ultimate load (KN)		Variation (%)
	FEA	Experimental tests	
S1'	10.7	9.3	86
S2'	11.7	9.3	79.5

Table 5: Comparison of deflection values between experimental and FEA results at ultimate load

Specimen	Deflection (mm)		Variation (%)
	FEA	Experimental tests	
S1'	134	132	98.6
S2'	125	121	96.8

7. Conclusions

1. Bolted connections have a slight advantage over the screw-fastened connections as it gives better connection capacity and ductility behavior.

2. However there is deference between the screw diameter and the bolt diameter there is no difference between failure modes as the failure was in the gusset plate.

3. Increasing the gusset plate thickness increase the ultimate load could be carried by the connection, moreover,

increasing the gusset plate thickness decreases the displacement made by the connection.

8. Acknowledgments

I would like to express my profound thanks to EMCON for their great assistance in the fabrication and installation of the specimens, as well as to HBRC, where all the experimental studies were carried out.

References

[1] Ye, J., Mojtabaei, S. M., & Hajirasouliha, I. (2018). Local-flexural interactive buckling of standard and optimised cold-formed steel columns. Journal of constructional steel research, 144, 106-118.

[2] Ye, J., Becque, J., Hajirasouliha, I., Mojtabaei, S. M., & Lim, J. B. (2018). Development of optimum cold-formed steel sections for maximum energy dissipation in uniaxial bending. Engineering structures, 161, 55-67.

[3] Rasmussen, K. J., & Zhang, H. (2019). Design of cold-formed steel single C-section portal frames. Journal of constructional steel research, 162, 105722.

[4] Schafer, B. W. (2008). The direct strength method of cold-formed steel member design. Journal of constructional steel research, 64(7-8), 766-778.

[5] Schafer, B. W. (2019). Advances in the Direct Strength Method of cold-formed steel design. Thin-Walled Structures, 140, 533-541.

[6] K. Zbirohowski-Koscia (1967). Thin Walled Beams: From Theory to Practice, Crosby Lockwood.

[7] Bhavitha, E. B., Rosemol, K. G., & Teena, J. (2015). Comparative study on moment connections in cold formed steel sections with and without perforations. International Journal of Innovative Science, Engineering & Technology, 21, 478-481.

[8] Liu, Q., Yang, J., & Wang, F. (2015). Numerical simulation of sleeve connections for cold formed steel sigma sections. Engineering Structures, 100, 686-695.

[9] Ye, J., Mojtabaei, S. M., Hajirasouliha, I., & Pilakoutas, K. (2020). Efficient design of cold-formed steel bolted-moment connections for earthquake resistant frames. Thin-Walled Structures, 150.

[10] Hanna, M. T., El-Saadawy, M. M., M El-Mahdy, G., & Aly, E. H. (2018). Behavior of Beam to Column Cold-Formed Section Connections Subjected to Bending Moments.

[11] Serror, M. H., Hassan, E. M., & Mourad, S. A. (2016). Experimental study on the rotation capacity of cold-formed steel beams. Journal of constructional steel research, 121, 216-228.

[12] A. Baigent, G.J. Hancock (1982). The Strength of Cold-formed Portal Frames. In Sixth International Specialty Conference on Cold-formed Steel Structures, Missouri S&T

[13] Lim, J. B., & Nethercot, D. A. (2004). Finite element idealization of a cold-formed steel portal frame. Journal of structural engineering, 130(1), 78-94.

[14] Rinchen, R., & Rasmussen, K. J. (2020). Experiments on long-span cold-formed steel single C-section portal frames. Journal of Structural Engineering, 146(1), 04019187.

[15] Rasmussen, K. J. (2019). Numerical modelling of cold-formed steel single C-section portal frames. Journal of Constructional Steel Research, 158, 143-155.

[16] Dundu, M. (2012). Base connections of single cold-formed steel portal frames. Journal of constructional steel research, 78, 38-44.

[17] El-Hadary, M. R., El-Aghoury, I. M., & Ibrahim, S. A. B. (2021). Behavior of different bolted connection configurations in frames composed of cold-formed sections. Ain Shams Engineering Journal.

[18] Rasmussen, K. J. (2019). Behaviour and modelling of connections in cold-formed steel single C-section portal frames. Thin-Walled Structures, 143, 106233.

[19] Smith M. ABAQUS/standard User's manual, version 2017. Providence, RI: Simulia; 2017.

[20] Wrzesien, A. M., Lim, J. B., Xu, Y., MacLeod, I. A., & Lawson, R. M. (2015). Effect of stressed skin action on the behaviour of cold-formed steel portal frames. Engineering Structures, 105, 123-136.